THE JOURNAL OF BIOLOGICAL CHEMISTRY VOL. 286, NO. 8, pp. 5942–5955, February 25, 2011


# Andrographolide Enhances Nuclear Factor-κB Subunit p65 Ser$^{536}$ Dephosphorylation through Activation of Protein Phosphatase 2A in Vascular Smooth Muscle Cells*

Received for publication, March 16, 2010, and in revised form, November 25, 2010 Published, JBC Papers in Press, December 17, 2010, DOI 10.1074/jbc.M110.123968

**Cheng Y. Hsieh[‡1], Ming J. Hsu[‡§1], George Hsiao[‡§], Yi H. Wang[‡¶], Chi W. Huang[‡], Shiuan W. Chen[‡], Thanasekaran Jayakumar[‡], Pei T. Chiu[§], Yi H. Chiu[‖], and Joen R. Sheu[‡§2]**

*From the [‡]Graduate Institute of Medical Sciences, Department of Pharmacology, the [§]School of Medicine, College of Medicine, and the [‖]Instrument Center, Office of Research and Development, Taipei Medical University, Taipei 11031, Taiwan and the [¶]Institute of Law and Interdiscipline, National Chengchi University, Taipei 11605, Taiwan*

**Recent studies have demonstrated that transcription factor nuclear factor (NF)-κB inhibition may contribute to the protective anti-inflammatory actions of andrographolide, an abundant component of plants of the genus *Andrographis*. However, the precise mechanism by which andrographolide inhibits NF-κB signaling remains unclear. We thus investigated the mechanism involved in andrographolide suppression of NF-κB signaling in rat vascular smooth muscle cells (VSMCs) exposed to proinflammatory stimuli, LPS, and IFN-γ. Andrographolide was shown to suppress LPS/IFN-γ-induced inducible nitric-oxide synthase and matrix metalloprotease 9 expression in rat VSMCs. Andrographolide also inhibited LPS/IFN-γ-induced p65 nuclear translocation, DNA binding activity, p65 Ser$^{536}$ phosphorylation, and NF-κB reporter activity. However, IKK phosphorylation and downstream inhibitory κBα phosphorylation and degradation were not altered by the presence of andrographolide in LPS/IFN-γ-stimulated VSMCs. These andrographolide inhibitory actions could be prevented by selective inhibition of neutral sphingomyelinase and protein phosphatase 2A (PP2A). Furthermore, andrographolide was demonstrated to increase ceramide formation and PP2A activity in VSMCs and to inhibit neointimal formation in rat carotid injury models. These results suggest that andrographolide caused neutral sphingomyelinase-mediated ceramide formation and PP2A activation to dephosphorylate p65 Ser$^{536}$, leading to NF-κB inactivation and subsequent inducible nitric-oxide synthase down-regulation in rat VSMCs stimulated by LPS and IFN-γ.**

The vascular inflammatory response involves complicated interactions among immunomodulatory cells, endothelial cells, and vascular smooth muscle cells (VSMCs).[3] Persistent increases in inflammatory cytokines derived from immune cells, endothelial cells, and VSMCs have been implicated in vascular dysfunction and vascular diseases, such as atherosclerosis, abdominal aortic aneurysms, and hypertension. These cytokines, including tumor necrosis factors (TNFs), interleukins (ILs), and interferons (IFNs), interact with specific receptors and activate signaling cascades leading to a variety of inflammatory responses involving matrix metalloproteinase (MMP) expressions, nitric oxide (NO) and reactive oxygen species production, and subsequent cell growth, adhesion, and migration (1, 2). In addition, there is increasing evidence from animal models that pattern recognition receptors (*i.e.* toll-like receptor 4 (TLR4)) mediate various inflammatory diseases in the cardiovascular system, including sepsis, septic shock, and atherosclerosis (3). In sepsis, the vascular endothelium barrier function becomes damaged and is lost (4). The underlying vascular smooth muscle is thus exposed and activated by pathogens, resulting in the induction of inducible nitric-oxide synthase (iNOS) and other inflammatory genes, leading to vascular collapse (5). In addition to its bactericidal function, NO derived from iNOS also acts as a potent vasodilator, which facilitates the mobilization of leukocytes into sites of infection (6). Although NO production is crucial for host defense, overproduction of NO can disrupt the circulatory system and cause vasculature injury, leading to multiorgan failure (7). NO derived from VSMCs is also known to contribute to the process of vascular diseases, such as atherosclerosis (8). Vascular inflammatory responses induced by pathogens or cytokines are accompanied by the generation of peroxynitrite, a potent and vasotoxic molecule formed from the reaction of NO and superoxide (9). Pharmacological approaches to diminish the effects of cytokines and pathogens may provide new strategies for managing inflammatory vascular diseases.

*Angrographis paniculae* has long been widely used in oriental medicine to alleviate inflammatory disorders. Andrographolide, a major component isolated from the leaves of *A. paniculae*, is thus expected to have anti-inflammatory pharmacological activities. Recent studies demonstrated that andrographolide possesses anticancer, hepatoprotective (10), and anti-inflammatory activities. Andrographolide was reported to suppress v-Src transformation and sensitize cancer cells to TNF-related apoptosis-inducing ligand-induced apo-

* This work was supported by National Science Council of Taiwan Grants NSC93-2321-B-038-001, 94-2321-B-038-001, and 97-2320-B-038-016-MY3.
[1] Both authors contributed equally to this work.
[2] To whom correspondence should be addressed: No. 250 Wu-hsing St., Taipei 11031, Taiwan. Tel.: 886-2-27361661 (ext. 3199); Fax: 886-2-27390450; E-mail: sheujr@tmu.edu.tw.
[3] The abbreviations used are: VSMC, vascular smooth muscle cell; iNOS, inducible nitric-oxide synthase; MMP, matrix metalloprotease; PP2A, protein phosphatase 2A; IKK, IκB kinase; 3-OMe-SM, 3-*O*-methyl-sphingomyeline; NRE, NF-κB response element; MTT, 3-(4,5-dimethylthiazol-2-yl)-2,5-diphenyl tetrazolium bromide; luc, luciferase; nSMase, neutral sphingomyelinase.

ptosis (11). Andrographolide was also shown to interfere with T-cell activation and dendritic cell maturation (12). In addition, andrographolide inhibits LPS-induced iNOS expression and subsequent NO production in macrophages (13). Bao *et al.* (14) also demonstrated the anti-inflammatory role of andrographolide in an ovalbumin-induced allergic lung inflammation model. The precise mechanism of andrographolide's attenuation of inflammatory responses has not been fully established. Activation of the nuclear factor (NF)-κB signaling cascade is currently known to play a causal role in host defense and inflammation. Several lines of evidence demonstrated that inhibition of NF-κB transcriptional activity contributes to andrographolide's protective anti-inflammatory actions (14–16). Moreover, andrographolide may covalently conjugate reduced cysteine 62 of the p50 subunit of NF-κB, leading to inhibition of nuclear NF-κB transcriptional activity (15). Whether andrographolide affects iNOS expression in VSMCs under vascular inflammatory conditions has not been reported. Previous studies demonstrated that iNOS expression is increased in VSMCs after exposure to the bacterial endotoxin, lipopolysaccharide (LPS), or cytokines (17). Moreover, the effect of LPS on iNOS expression is strengthened by the combination of one or more cytokines (18). We thus investigated the protective effects of andrographolide on iNOS expression in rat VSMCs co-stimulated by LPS and IFN-γ, which represents a vascular inflammatory condition.

## EXPERIMENTAL PROCEDURES

*Reagents*—Andrographolide and LPS were purchased from Sigma. Recombinant rat INF-γ was purchased from Peprotech (Rocky Hill, NJ). Okadaic acid was obtained from Calbiochem. 3-*O*-Methyl-sphingomyeline (3-OMe-SM) was purchased from Biomol (Plymouth Meeting, PA). C16:0 ceramide, C17:0 ceramide, C18:0 ceramide, C24:0 ceramide, and C24:1 ceramide were all purchased from Avanti Polar Lipids, Inc. (Alabaster, AL). Dulbecco's modified Eagle's medium (DMEM), fetal calf serum (FCS), and penicillin/streptomycin were purchased from Invitrogen. Antibodies specific for α-tubulin and iNOS were purchased from Transduction Laboratories (Lexington, KY). Antibodies specific for p65 (c-Rel), HDAC3, MMP-9, and anti-mouse and anti-rabbit immunoglobulin G (IgG)-conjugated horseradish peroxidase (HRP) antibodies were purchased from Santa Cruz Biotechnology, Inc. (Santa Cruz, CA). Antibodies specific for IκBα, IKK phosphorylated at $Ser^{180}/Ser^{181}$, IκBα phosphorylated at $Ser^{32}/Ser^{36}$, and p65 phosphorylated at $Ser^{276}/Ser^{536}$ were purchased from Cell Signaling (St. Louis, MO). A light shift chemiluminescent EMSA kit was purchased from Pierce. The reporter plasmid, NFκB-Luc was purchased from Clontech (Mountain View, CA). The *Renilla*-luc and Dual-Glo luciferase assay systems were purchased from Promega (Madison, WI). All materials for immunoblotting were purchased from Bio-Rad. All other chemicals were obtained from Sigma.

*Rat Aortic SMC Primary Culture*—Male Wistar rats used in this study were purchased from BioLASCO (Taipei, Taiwan). VSMCs were enzymatically dispersed from male Wistar rats (250–300 g). Thoracic aortas from Wistar rats were removed and stripped of endothelium and adventitia. VSMCs were obtained by a modification of the combined collagenase and elastase digestion method (17). These cells were grown in DMEM supplemented with 20 mM HEPES, 10% fetal bovine serum (FBS), 1% penicillin/streptomycin, and 2 mM glutamine at 37 °C in a humidified atmosphere of 5% $CO_2$. The growth medium was changed every 2–3 days until cells had reached confluence. The growth medium was removed, and the monolayer was rinsed with phosphate-buffered saline (PBS). A trypsin-EDTA solution was added, and the monolayer was incubated at 37 °C for 2 min. The culture dishes were observed under a phase-contrast microscope until the cells had detached. Cells were removed with 10 ml of DMEM and centrifuged at 900 × *g* for 7 min. The pellet was resuspended in DMEM in a culture dish, and cells from passages 4–8 were used in all experiments. Primary cultured rat aortic VSMCs showed the "hills and valleys" pattern, and the expression of α-smooth muscle actin was confirmed (data not shown). All protocols were approved by the Taipei Medical University Animal Care and Use Committee.

*Cell Viability Assay*—Cell viability was measured by the colorimetric 3-(4,5-dimethylthiazol-2-yl)-2,5-diphenyl tetrazolium bromide (MTT) assay as described previously (19).

*Determination of Nitrite Concentrations*—To determine NO production, nitrite, a stable oxidative end product of NO, was measured using the colorimetric method as described previously (17). Nitrite accumulation was determined via a colorimetric reaction based on the Griess reagent (1% sulfanilamide and 0.1% naphthylenediamine in 2.5% phosphoric acid). The optical absorbance at 550 nm was measured with a microplate reader (MRX microplate reader). Nitrite concentrations were calculated by regression with standard solutions of sodium nitrite prepared in the same culture medium.

*Reverse Transcription (RT)-PCR*—Total RNA was isolated from cells using the TRIzol reagent (Invitrogen) as described previously (17). RT-PCR was then conducted following the manufacturer's instructions (SuperScript One-step RT-PCR system, Invitrogen). Primers used for amplification of the iNOS and GAPDH fragments were as follows: iNOS, sense (5′-ACCTACTTCCTGGACATCAC-3′) and antisense (5′-ACCCAAACACCAAGGTCATG-3′); GAPDH, sense (5′-GCCGCCTGGTCACCAGGGCTG-3′) and antisense (5′-ATGGACTGTGGTCATGAGCCC-3′). GAPDH was used as an internal control. PCR products were run on agarose gel, stained with ethidium bromide, and visualized by UV illumination.

*Immunoblot Analysis*—Immunoblot analyses were performed as described previously (17). Briefly, cells were lysed in extraction buffer containing 10 mM Tris (pH 7.0), 140 mM NaCl, 2 mM PMSF, 5 mM DTT, 0.5% Nonidet P-40, 0.05 mM pepstatin A, and 0.2 mM leupeptin. Samples of equal amounts of protein were subjected to SDS-PAGE and transferred onto a polyvinylidene fluoride (PVDF) microporous membrane, which was then incubated in TBST buffer (150 mM NaCl, 20 mM Tris-HCl, and 0.02% Tween 20, pH 7.4) containing 5% nonfat milk. Proteins were visualized by specific primary antibodies and then incubated with HRP-conjugated secondary antibodies. Immunoreactivity was detected using enhanced chemiluminescence (ECL) following the manufacturer's in-

structions. Quantitative data were obtained using a computing densitometer with a scientific imaging system (Eastman Kodak Co.).

*Gelatin Zymography*—Culture media harvested from cells were analyzed for proteins with gelatinolytic activity by gelatin zymography. Briefly, 10-μl aliquots of conditioned media were resuspended in non-reducing sample buffer and applied to 10% SDS-PAGE copolymerized with gelatin (1%). After electrophoresis, gels were washed with 2.5% Triton X-100 for 1 h and subsequently incubated in enzyme buffer (50 mM Tris-HCl (pH 7.5), 20 mM NaCl, 5 mM $CaCl_2$, and 0.02% Brij-35) at 37 °C for 72 h. Gels were then stained with 0.5% Coomassie Brilliant Blue G-250. Following destaining in 25% methanol and 10% acetic acid, proteins with gelatinolytic activity were visualized as clear bands against a blue-stained background. Gels were scanned, and a densitometric analysis was performed using the image analysis program Quantity One (Bio-Rad). Molecular sizes of the bands were characterized by comparison with prestained molecular weight markers.

*PP2A Activity Assay*—An immunoprecipitation phosphatase assay kit (Millipore, Billerica, MA) was used to measure phosphate release as an index of phosphatase activity according to the manufacturer's instructions. Briefly, 200 μg of cellular proteins was immunoprecipitated with a mouse anti-PP2A catalytic subunit antibody (1 μg/μl; Millipore) and incubated with substrate, phosphoprotein (amino acid sequence KRpTIRR, 750 μM), in protein phosphatase assay buffer (20 mM 4-morpholinepropanesulfonic acid (pH 7.5), 60 mM 2-mercaptoethanol, 0.1 M NaCl, and 0.1 mg/ml serum albumin). Reactions were initiated by the addition of the phosphoprotein substrate and carried out for 10 min at 30 °C. Reactions were terminated by the addition of 100 μl of the malachite green solution. The absorbance at 650 nm was measured on a microplate reader.

*Preparation of Nuclear Extracts and Oligonucleotide Pull-down Assay*—The cytosolic and nuclear protein fractions were separated as described previously (20). Briefly, cells were lysed in hypotonic buffer (10 mM HEPES (pH 7.9), 10 mM KCl, 0.5 mM DTT, 10 mM aprotinin, 10 mM leupeptin, and 20 mM PMSF) for 15 min on ice and vortexed for 10 s. Nuclei were pelleted by centrifugation at 15,000 × *g* for 1 min. A pellet containing nuclei was resuspended in hypertonic buffer (20 mM HEPES (pH 7.6), 25% glycerol, 1.5 mM $MgCl_2$, 4 mM EDTA, 0.05 mM DTT, 10 mM aprotinin, 10 mM leupeptin, and 20 mM PMSF) for 30 min on ice. Supernatants containing nuclear proteins were collected by centrifugation at 15,000 × *g* for 2 min, and the oligonucleotide pull-down assay was then performed. Briefly, nuclear proteins (10 μg) were incubated at 30 °C for 60 min with 0.5 nmol of 5′-biotinylated double-stranded wild-type (5′-AGTTGAGGGGACTTTCCCAGG-3′) or mutant (5′-CAGTAGTATGTGAGCCTGCCA-3′) oligonucleotides, coupled previously to streptavidin-agarose beads (Sigma). The wild-type oligonucleotide corresponded to the nuclear cognate NF-κB binding sequence (NF-κB response element; NRE). After incubation, the biotinylated oligonucleotide-coupled streptavidin beads were washed three times with hypotonic buffer and denatured in SDS-sample buffer. The samples were subjected to immunoblotting analysis for p65 using specific antibodies.

*Transfection and NF-κB-Luciferase Assays*—Cells ($2 \times 10^5$/well) were transfected with κB-luc plus *Renilla*-luc using Lipofectamine reagent (Invitrogen). Cells with or without treatments were then harvested, and the luciferase activity was determined using a Dual-Glo luciferase assay system kit (Promega) and was normalized on the basis of *Renilla* luciferase activity. The level of induction of luciferase activity was compared as the ratio of cells with and without LPS/IFN-γ stimulation.

*Suppression of pp2a Expression*—Protocol for target gene suppression was described previously (20). For *pp2a* suppression, predesigned siRNAs targeting the mouse *pp2a* gene were purchased from Ambion (Austin, TX). The siRNA oligonucleotide targeting the coding regions of mouse PP2A catalytic subunit (PP2A-C) mRNA was as follows: *pp2a* siRNA, 5′-ccauacuccgagggaaucatt-3′. The negative control siRNA comprising a 19-bp scrambled sequence with 3′dT overhangs was also purchased from Ambion.

*Quantification of Ceramide*—The quantification of ceramide in VSMCs was performed as described previously (21). VSMCs were cultured in 10-cm dishes until a required confluence was reached. Cells were treated with andrographolide for the indicated times and then washed twice in ice-cold PBS and collected in 0.5 ml of PBS. Cells were pelleted by centrifugation at 2,000 rpm for 5 min, and the lipids were extracted using 500 μl of methanol after the addition of internal standards (C17:0 ceramide). The suspension was incubated at 25 °C for 30 min with constant shaking and then centrifuged at 25,000 rpm for 30 min at 25 °C. The supernatants were collected, and the extraction was repeated three times. The combined organic phases of supernatants was utilized for the estimation of ceramide. The liquid-liquid extractions; the amounts of C16:0 ceramide, C18:0 ceramide, C24:0 ceramide, and C24:1 ceramide; and the internal standards were determined by liquid chromatography coupled with tandem mass spectrometry. Chromatographic separation was accomplished under gradient conditions using a Luna C18 column (150 × 2-mm inner diameter, 5-μm particle size, and 10-nm pore size). The HPLC mobile phase consisted of water/formic acid (100 ml:0.1 ml) (A) and acetonitrile/tetrahydrofuranformic acid (50 ml:0.1 ml) (B). A gradient program was used for the HPLC separation at a flow rate of 0.3 ml/min. The initial buffer composition was 60% (A), 40% (B) and held for 0.6 min and then linearly changed to 0% (A), 100% (B) in 4.4 min and held for 5 min, and then linearly returned to 60% (A), 40% (B) in 0.5 min and held for an additional 5.5 min. Each 40 μl of samples was injected with the total run time of 16 min. Tandem mass spectrometry analyses were performed on an API 4,000 triple quadrupole mass spectrometer with a Turbo V source (Applied Biosystems, Darmstadt, Germany). Precursor-to-product ion transitions of $m/z$ 536.8 → 280.5 for C16:0 ceramide, $m/z$ 564.9 → 308.5 for C18:0 ceramide, $m/z$ 646.9 → 390.8 for C24:1 ceramide, $m/z$ 648.9 → 392.8 for C24:0 ceramide, and $m/z$ 550.9 → 294.5 for C17:0 ceramide were used for multiple reaction monitoring with a well time of 15 ms. Concentrations of the calibration standards, quality con-

trols, and unknowns were evaluated by Analyst software version 1.4.2 (Applied Biosystems). The mean peak areas of the samples reconstructed with internal standards were compared with the mean peak area of 10 ng/ml internal standards in methanol. Total ceramide was calculated from the sum of C16:0, C18:0, C24:0, and C24:1 ceramide subspecies.

*Rat Carotid Balloon Angioplasty*—Male Wistar rats (350–400 g) were anesthetized with chloral hydrate (0.4 g/kg intraperitoneal) and a 2F embolectomy balloon catheter (2F, Forgarty, Edwards Lifesciences, Irvine, CA) introduced into the right common carotid artery via the external artery. The balloon was inflated to distend the common carotid artery and was then withdrawn to the external artery. This procedure was repeated three times, the catheter was then removed, and the distal external artery segment was ligated. The animals were divided into two groups: 1) an untreated group and 2) an andrographolide treatment group (5 mg/kg/day for 2 weeks). A miniosmotic pump (model 2002, Alza (Palo Alto, CA)) with a pump rate of 0.5 $\mu$l/h containing sufficient solution for 14 days was filled with andrographolide in DMSO and implanted subcutaneously on the back of the neck. Fourteen days after balloon angioplasty, the rats were anesthetized and perfused with saline. The right common carotid artery was isolated then cut into 5-$\mu$m sections, stained with hematoxylin and eosin, and photographed through a microscope (Nikon Eclipse TS100, Nikon, Tokyo, Japan), and the neointimal areas were measured by the Image-Pro Express 6.0 system (Media Cybernetics Inc., Bethesda, MD). The medial area was calculated by subtracting the internal elastic lamina from the external elastic lamina, and the intimal area was calculated by subtracting the lumen area from the internal elastic lamina. From these measurements, the ratio of intimal area and medial area was calculated. Arterial tissues were also obtained from the sacrificed animals and immediately snap-frozen. These tissues were homogenized in ice-cold lysis buffer and subjected to immunoblotting to determine the levels of iNOS.

*Statistical Analysis*—Results are presented as means ± S.E. from at least three independent experiments. One-way analysis of variance followed by, when appropriate, the Newman-Keuls test was used to determine the statistical significance of the difference between means. A $p$ value of $<0.05$ was considered statistically significant.

## RESULTS

*Effects of Andrographolide on LPS/IFN-γ-induced iNOS and MMP-9 Expressions*—To examine whether andrographolide affects NO formation in VSMCs exposed to LPS and IFN-γ, the level of nitrite, an end product of NO, was determined. As shown in Fig. 1*A*, treatment of rat VSMCs with the combination of LPS (50 $\mu$g/ml) and IFN-γ (100 units/ml) for 24 h significantly induced NO production from 0.4 ± 0.1 to 5.9 ± 0.5 $\mu$M ($n = 4$). We thus used these concentrations of LPS (50 $\mu$g/ml) and IFN-γ (100 units/ml) in the following experiments, represented as LPS/IFN-γ. Andrographolide at the concentrations of 20 and 50 $\mu$M significantly inhibited LPS/IFN-γ-induced NO production in rat VSMCs by 62.8 ± 6.1% and 79.8 ± 2.3%, respectively. We next examined whether the protein level of iNOS, which catalyzes NO formation, was affected by andrographolide in LPS/IFN-γ-stimulated cells. As shown in Fig. 1*B*, LPS/IFN-γ markedly increased iNOS expression as compared with the control group. The compiled data are shown at the *bottom* of Fig. 1*B* (LPS/IFN-γ, 8.1 ± 0.2-fold; control, 1.0 ± 0.0-fold; $p < 0.05$). LPS/IFN-γ-induced iNOS expression was suppressed by the presence of andrographolide (Fig. 1*B*) (LPS/IFN-γ, 8.1 ± 0.2-fold; LPS/IFN-γ plus 20 $\mu$M andrographolide, 4.8 ± 0.2-fold; LPS/IFN-γ plus 50 $\mu$M andrographolide, 3.9 ± 0.6-fold; $p < 0.05$). RT-PCR analysis was then used to confirm the hypothesis that andrographolide's attenuation of LPS/IFN-γ-induced iNOS expression was accompanied by a decrease in iNOS mRNA. LPS/IFN-γ significantly induced iNOS mRNA elevation by 22.2 ± 2.1-fold in rat VSMCs after 12 h of treatment as compared with the control group (Fig. 1*C*). In addition, andrographolide at the concentrations of 20 and 50 $\mu$M significantly reduced LPS/IFN-γ-increased iNOS mRNA by 29.6 ± 8.8% and 81.6 ± 1.8%, respectively. These results suggest that andrographolide's inhibition of LPS/IFN-γ-induced NO formation may have resulted from transcriptional down-regulation of iNOS. Under a vascular inflammatory state, cytokine activation of VSMCs can also increase the production and processing of MMPs from inactive zymogens to active enzymes (22). Activated MMPs digesting the vascular extracellular matrix, resulting in a weakening and dilatation of the aortic wall is a hallmark of the pathogenesis of vascular inflammatory diseases. Excess degradation of the extracellular matrix by MMPs may also contribute to VSMC migration and proliferation (23). We then attempted to elucidate whether andrographolide regulates the activities of MMP-2 and MMP-9 in LPS/IFN-γ-treated rat VSMCs. Results from Fig. 1*D* demonstrate that andrographolide significantly inhibited LPS/IFN-γ-increased MMP-9 activity in rat VSMCs as determined by a zymographic analysis (Fig. 1*D*) (control, 1.0 ± 0.0-fold; LPS/IFN-γ, 4.5 ± 0.9-fold; LPS/IFN-γ plus 20 $\mu$M andrographolide, 2.5 ± 0.7-fold; LPS/IFN-γ plus 50 $\mu$M andrographolide, 1.6 ± 0.4-fold). In contrast, andrographolide had no effect on MMP-2 activity in the absence or presence of LPS and IFN-γ (Fig. 1*D*). The immunoblot analysis shown in Fig. 1*E* further demonstrated that andrographolide suppressed the increase in the MMP-9 protein level in cells exposed to LPS and IFN-γ. To further determine whether the cytotoxic effect was attributable to andrographolide's actions in LPS/IFN-γ-treated rat VSMCs, an MTT assay was employed. As shown in Fig. 1*F*, treatment of cells with andrographolide at concentrations of 20 or 50 $\mu$M for 24 h did not alter cell viability. These findings together suggested that andrographolide may inhibit LPS/IFN-γ-induced vascular inflammatory responses, including increasing iNOS expression and subsequent NO formation and elevating MMP-9 activity in rat VSMCs.

*Effects of Andrographolide on NF-κB Activation in LPS/IFN-γ-stimulated Rat VSMCs*—To clarify the mechanism of MMP-9 and iNOS inhibition by andrographolide, we examined the status of NF-κB activation, a well known transcriptional factor for driving gene expression of many inflammatory proteins, including MMP-9 and iNOS (24, 25). The

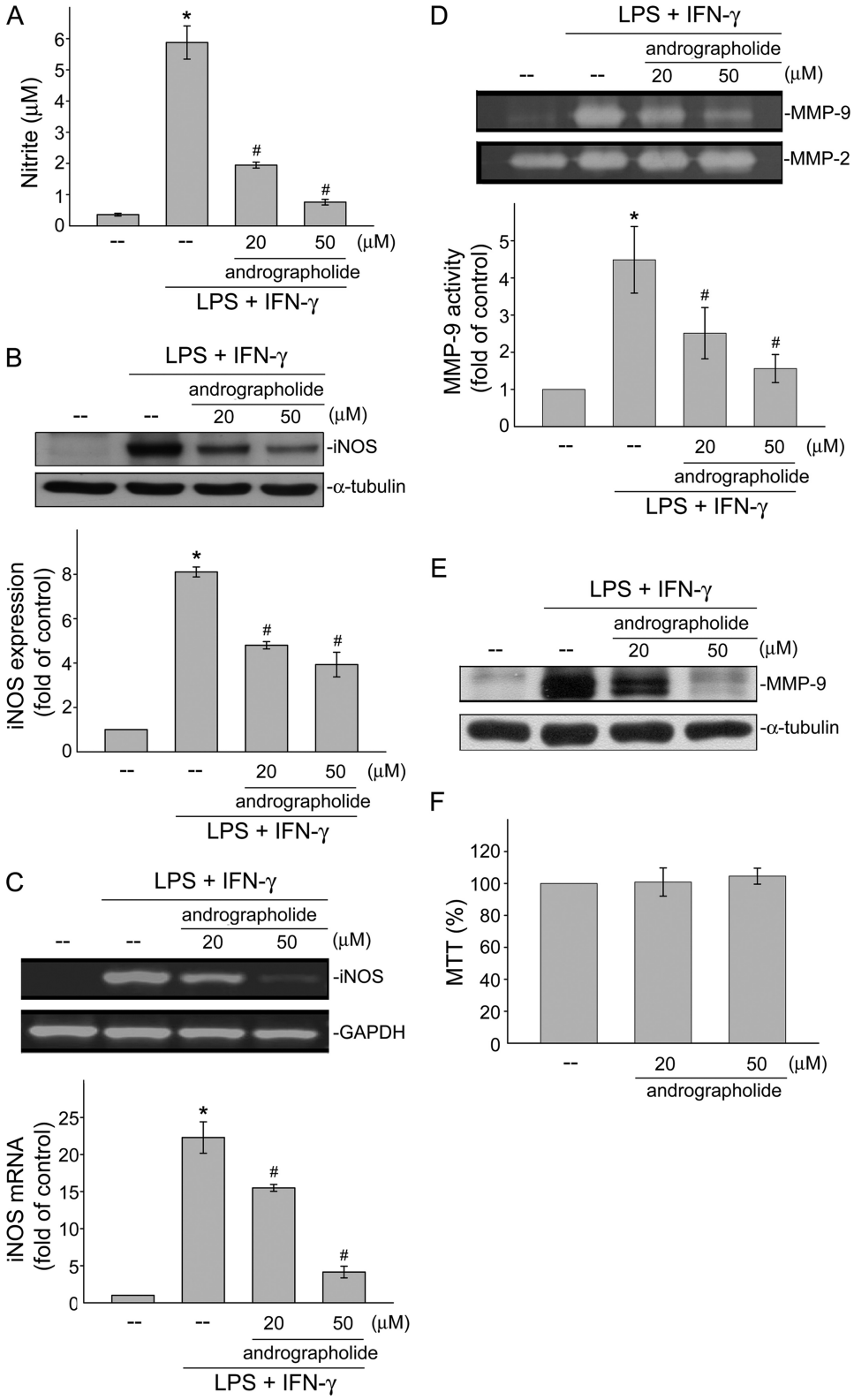


FIGURE 1. **Effects of andrographolide on LPS/IFN-γ-induced iNOS and MMP-9 expressions.** Rat VSMCs were pretreated with vehicle or 20 or 50 μM andrographolide for 30 min before treatment with the combination of LPS (50 μg/ml) and IFN-γ (100 units/ml) for another 12 h (*C*) or 24 h (*A*, *B*, and *D–F*). Nitrite concentrations (*A*), iNOS protein level (*B*), iNOS mRNA (*C*), MMP-2 and MMP-9 activities (*D*), and MMP-9 expression (*E*) were then determined. *F*, cell viability in cells exposed to andrographolide was determined by MTT assay. Data (*A*, *B–D*, and *F*) are presented as means ± S.E. (*error bars*). *, $p < 0.05$, compared with the control group; #, $p < 0.05$, compared with the vehicle-treated group in the presence of LPS/IFN-γ. Data shown in *E* are representative of three separate experiments with similar results.

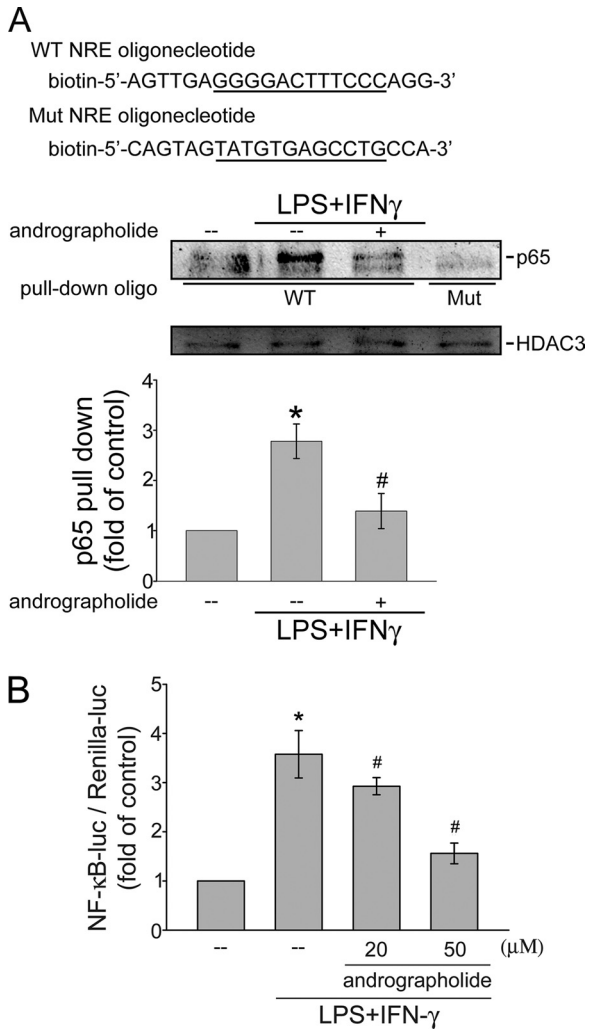


FIGURE 2. **Effects of andrographolide on NF-κB activation in LPS/IFN-γ-stimulated rat VSMCs.** *A*, cells were pretreated with vehicle or andrographolide for 30 min before treatment with the combination of LPS (50 μg/ml) and IFN-γ (100 units/ml) for another 30 min. Following incubation, the nuclear protein fraction was prepared for the oligonucleotide pull-down assay. The input extracts were normalized between samples by analyzing the levels of HDAC3. Data are presented as means ± S.E. (*error bars*). *, $p < 0.05$, compared with the control group; #, $p < 0.05$, compared with the vehicle-treated group in the presence of LPS/IFN-γ. *B*, cells were transiently transfected with NF-κB-luc and *Renilla*-luc for 24 h. After transfection, cells were pretreated with vehicle or andrographolide for 30 min before treatment with the combination of LPS (50 μg/ml) and IFN-γ (100 units/ml) for another 24 h. An NF-κB-luciferase assay was then carried out. Data represent means ± S.E. of three independent experiments performed in duplicate. *, $p < 0.05$, compared with the control group; #, $p < 0.05$, compared with the vehicle-treated group in the presence of LPS/IFN-γ. *Mut*, mutant.

nuclear extracts of rat VSMCs with or without andrographolide treatment were subjected to an oligonucleotide pull-down assay. To demonstrate physical interaction of NF-κB/p65 with the NF-κB-binding sequence, we used biotinylated, double-stranded oligonucleotides coupled to streptavidin-agarose beads (wild-type or mutant NRE) to pull down proteins interacting with the NF-κB-binding sequence in LPS/IFN-γ-stimulated rat VSMCs in the absence or presence of andrographolide. The bound protein complex was then analyzed by Western blotting. As shown in Fig. 2*A*, LPS/IFN-γ treatment increased the binding of p65 to the wild-type NRE oligonucleotide containing binding sequences for NF-κB. LPS/IFN-γ-induced p65 activation was attenuated by pretreatment of cells with 50 μM andrographolide for 30 min. However, p65 did not bind to a similar oligonucleotide with the mutation of the NF-κB-binding sequence after LPS/IFN-γ treatment, indicating that DNA-protein interactions were sequence-specific (Fig. 2*A*).

A reporter assay was then employed to directly determine andrographolide's attenuation of NF-κB transactivity in LPS/IFN-γ-stimulated cells. Cells were transiently transfected with a κB-luc reporter construct. As shown in Fig. 2*B*, cells treated with LPS/IFN-γ for 24 h exhibited an increase in NF-κB-luciferase activity. The increase in NF-κB-luciferase activity was 3.6 ± 0.5-fold as compared with the control group ($n = 3$) after LPS/IFN-γ treatment. Furthermore, the LPS/IFN-γ-induced increase in NF-κB-luciferase activity was markedly suppressed by 16.4 ± 7.3% and 55.6 ± 6.9% in cells pretreated for 30 min with 20 and 50 μM andrographolide, respectively ($n = 3$) (Fig. 2*B*). These results suggest that andrographolide may reduce iNOS and MMP-9 expressions by suppressing NF-κB transactivity in rat VSMCs.

*Effects of Andrographolide on IκB Phosphorylation and Degradation in LPS/IFN-γ-stimulated Rat VSMCs*—NF-κB activity is tightly controlled by binding to the IκB inhibitor protein, which prevents cytosolic NF-κB from entering the nucleus. Once phosphorylated by the IκB kinase (IKK) complex, IκB dissociates from the NF-κB subunits, is ubiquitinated, and is rapidly degraded by the proteasome (26). IKK phosphorylation of the IκBα $Ser^{32}$ and $Ser^{36}$ residues was proposed as being a major mode for IκBα degradation, leading to NF-κB translocation and activation (27). We examined whether the extent of IκBα $Ser^{32}$ and $Ser^{36}$ phosphorylation is altered after LPS/IFN-γ exposure. LPS/IFN-γ caused a marked increase in IκBα phosphorylation at as early as 5 min, and this was sustained to 20 min after LPS/IFN-γ exposure (Fig. 3*A*). In parallel, the total amount of the IκB protein was dramatically decreased after exposure to LPS/IFN-γ for 20 min and had returned to a basal level after 60 min of treatment with LPS/IFN-γ (Fig. 3*B*). Treatment of cells with andrographolide only slightly affected LPS/IFN-γ-induced IκBα phosphorylation at $Ser^{32}$ and $Ser^{36}$ (Fig. 3*C*). Furthermore, andrographolide did not restore normal levels of IκBα in LPS/IFN-γ-stimulated cells (Fig. 3*D*). These results suggested that the IκBα phosphorylation and subsequent IκBα degradation in LPS/IFN-γ-stimulated cells might not contribute to andrographolide's inhibitory actions on NF-κB signaling.

*Effects of Andrographolide on IKK Phosphorylation and NF-κB Nuclear Translocation in LPS/IFN-γ-stimulated Rat VSMCs*—We next determined whether IKKs, including IKKα and IKKβ, critical upstream molecules of IκBα (27), contributed to andrographolide attenuation of LPS/IFN-γ-induced NF-κB activation. As shown in Fig. 4*A*, IKK phosphorylations at $Ser^{180}$ (IKKα) and $Ser^{181}$ (IKKβ) were significantly increased in LPS/IFN-γ-stimulated rat VSMCs. The compiled data are shown at the *bottom* of Fig. 4*A* (LPS/IFN-γ, 1.8 ± 0.3-fold; control, 1.0 ± 0.0-fold; $p < 0.05$). However, pretreatment of cells with 20 or 50 μM andrographolide did not significantly affect LPS/IFN-γ-induced IKK phosphorylation (Fig. 4*A*). Based on the findings above that andrographolide's at-

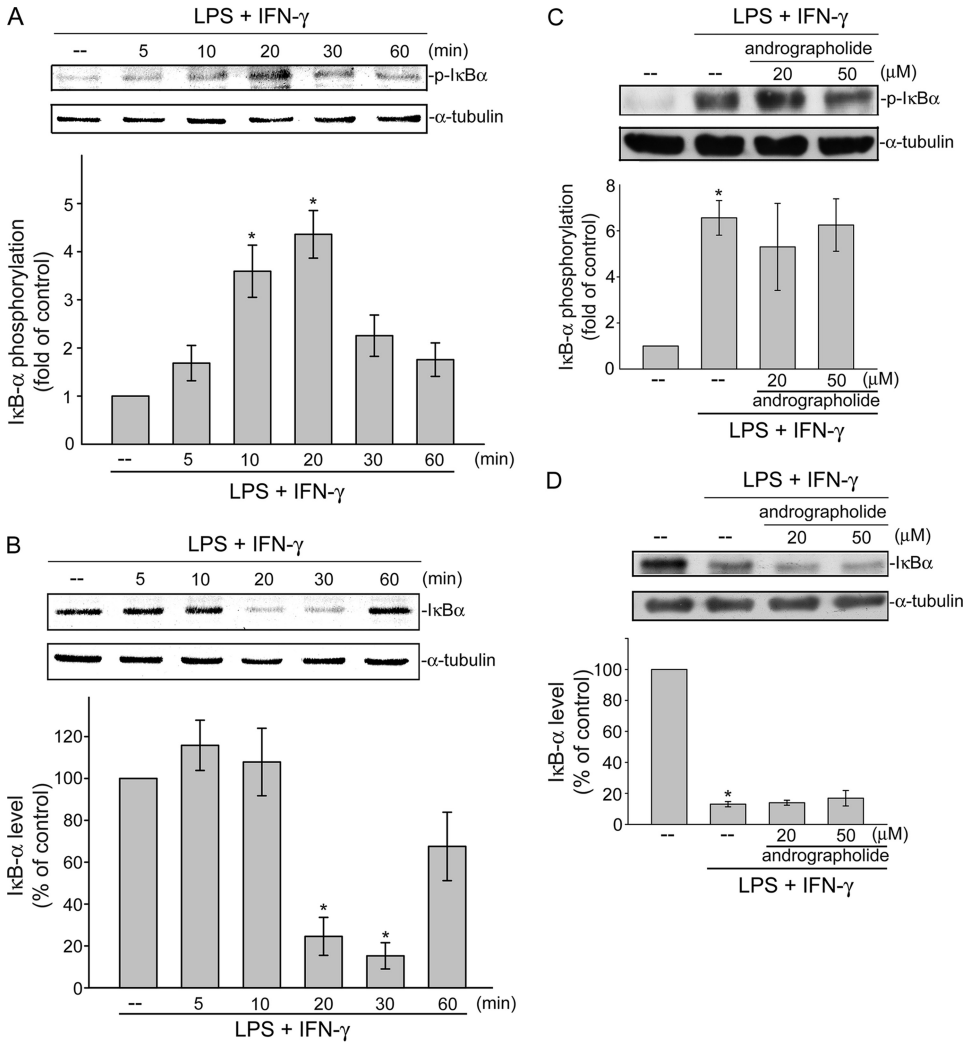


FIGURE 3. **Effects of andrographolide on IκB phosphorylation and degradation in LPS/IFN-γ-stimulated rat VSMCs.** Cells were treated with the combination of LPS (50 μg/ml) and IFN-γ (100 units/ml) for the indicated time periods. Cells were then harvested, and IκBα phosphorylation at $Ser^{32}/Ser^{36}$ (*A*) or IκBα level (*B*) was determined using immunoblotting. Cells were pretreated with vehicle or andrographolide for 30 min before treatment with the combination of LPS (50 μg/ml) and IFN-γ (100 units/ml) for another 30 min. After treatment, cells were harvested to assess the extent of IκBα phosphorylation (*C*) or IκBα level (*D*). Data are presented as means ± S.E. (*error bars*). *, $p < 0.05$, compared with the control group.

tenuation of NF-κB signaling might bypass its natural regulation through the IKK-IκBα cascade, we sought to examine whether andrographolide interferes with the NF-κB subcellular localization. NF-κB/p65 was shown to shuttle from the cytoplasm to nuclei after exposure to various inflammatory stimuli (28). Therefore, we analyzed p65 protein levels in cytoplasmic and nuclear fractions of LPS/IFN-γ-stimulated rat VSMCs. As shown in Fig. 4, *B* and *C*, p65 exhibited a decreased cytoplasmic localization (Fig. 4*B*) and increased nuclear localization (Fig. 4*C*) in cells that had been treated with LPS/IFN-γ. Pretreatment with andrographolide markedly impaired p65 translocation from cytosol to nucleus in cells exposed to LPS/IFN-γ (Fig. 4, *B* and *C*). Several studies demonstrated that phosphorylation of p65 at critical serine residues may account for its dimerization, DNA binding, and nuclear localization (29). Individual phosphorylation sites may be targeted by a single or by several kinases (27). Protein kinase A phosphorylation of p65 $Ser^{276}$ mediates dimerization and DNA binding of p65 (30). The phosphorylation of $Ser^{536}$ (31) following TNF and LPS stimulation increases p65 transcriptional activity. In order to identify phosphorylation events that may be critical in andrographolide regulation of NF-κB, we determined the status of p65 phosphorylation at $Ser^{276}$ and $Ser^{536}$. As shown in Fig. 4*D*, LPS/IFN-γ-induced p65 $Ser^{276}$ phosphorylation was not altered by the presence of andrographolide in rat VSMCs. In contrast, LPS/IFN-γ-induced p65 $Ser^{536}$ phosphorylation was significantly inhibited in cells pretreated for 30 min with 50 μM andrographolide by 76.2% ± 15.9%, respectively ($n = 3$) (Fig. 4*E*). These results suggest that p65 $Ser^{536}$ phosphorylation may be responsible for andrographolide's inhibition of NF-κB transactivation in LPS/IFN-γ-stimulated rat VSMCs.

*PP2A Is Involved in Andrographolide Attenuation of NF-κB Activity*—We next explored the mechanism by which andrographolide suppresses LPS/IFN-γ-induced p65 $Ser^{536}$ phosphorylation. The mechanism that regulates p65 $Ser^{536}$ dephosphorylation remains to be identified. Regulation of the phosphorylated protein is balanced by the activities of kinases and phosphatases (32). It is conceivable that andrographolide may activate a protein phosphatase that dephosphorylates

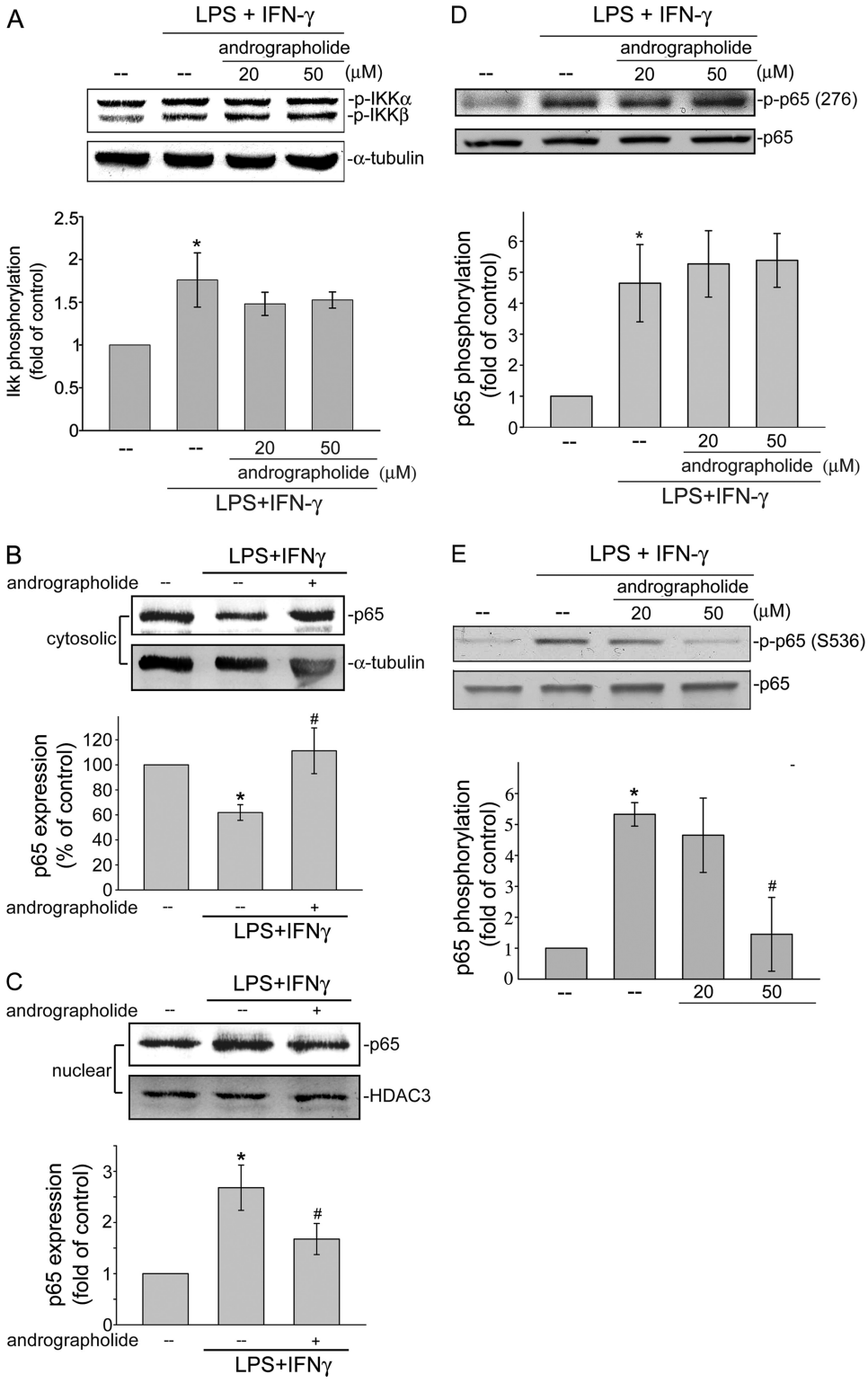


FIGURE 4. **Effects of andrographolide on IKK phosphorylation and NF-κB nuclear translocation in LPS/IFN-γ-stimulated rat VSMCs.** Cells were pretreated with vehicle or andrographolide for 30 min before treatment with the combination of LPS (50 μg/ml) and IFN-γ (100 units/ml) for another 30 min. The extent of IKKα/β phosphorylation (*A*), p65 levels in the cytosolic (*B*) and nuclear fractions (*C*), and the extent of p65 Ser$^{276}$ (*D*) or p65 Ser$^{536}$ phosphorylation (*E*) were then determined. Data are presented as means ± S.E. (*error bars*). *, $p < 0.05$, compared with the control group. #, $p < 0.05$, compared with the LPS/IFN-γ-treated group.

Ser$^{536}$, leading to NF-κB inactivation and iNOS down-regulation. Protein phosphatase 2A (PP2A) is a serine/threonine-specific protein phosphatase that regulates the activities of several major protein kinase families, such as ASK1 (20).

Thus, we attempted to determine whether PP2A is involved in p65 Ser$^{536}$ dephosphorylation in response to andrographolide in LPS/IFN-γ-stimulated rat VSMCs. Okadaic acid is a selective inhibitor of PP2A at low concentrations (1–10 nM)

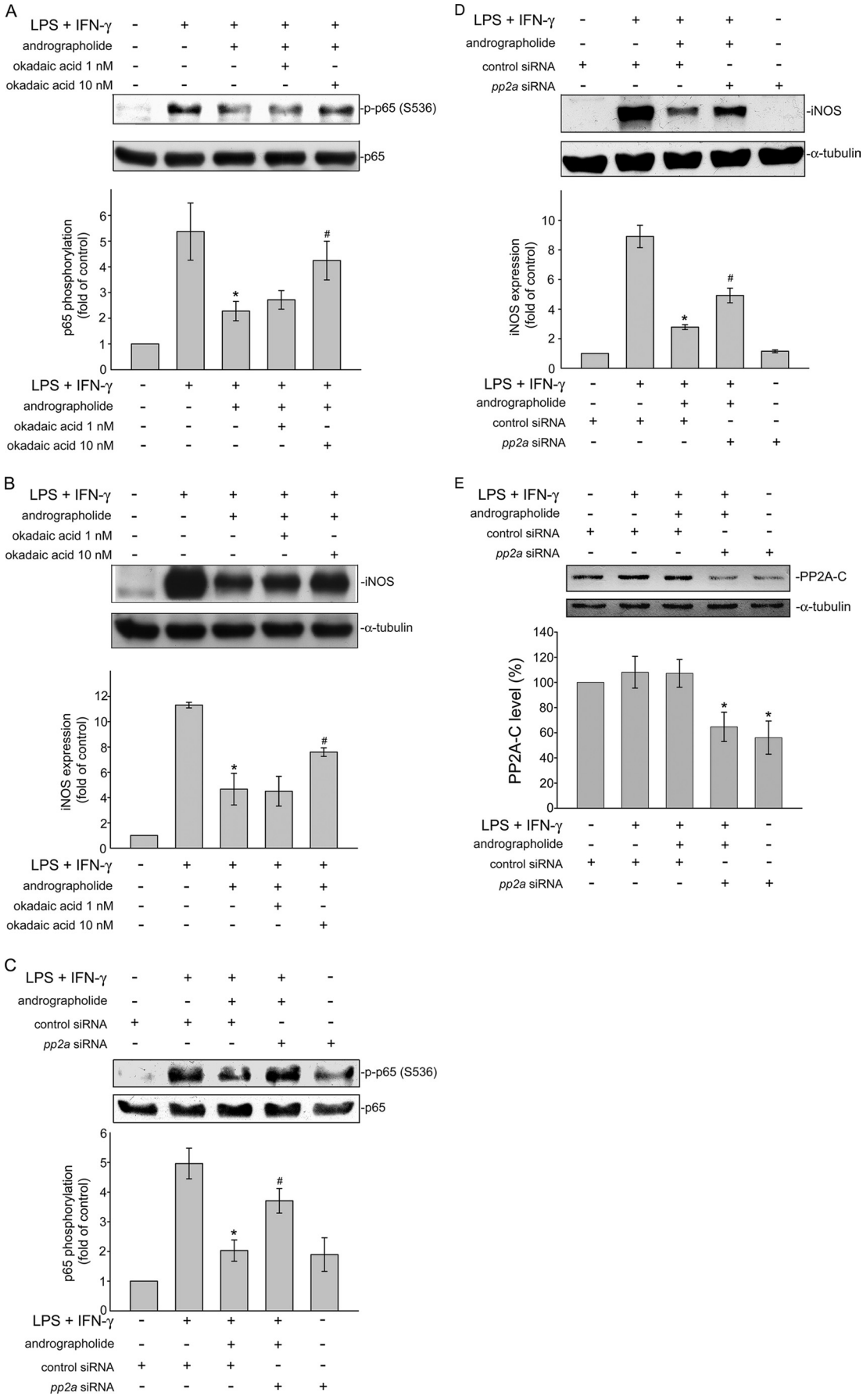
A
LPS + IFN-γ
andrographolide
okadaic acid 1 nM
okadaic acid 10 nM
-p-p65 (S536)
-p65
p65 phosphorylation (fold of control)
B
-iNOS
-α-tubulin
iNOS expression (fold of control)
C
control siRNA
pp2a siRNA
D
E
-PP2A-C
PP2A-C level (%)

but inhibits PP1 at much higher concentrations (20). As shown in Fig. 5*A*, pretreatment with okadaic acid for 30 min at a concentration of 10 nM significantly restored andrographolide inhibition of p65 Ser$^{536}$ phosphorylation in cells exposed to LPS/IFN-γ. In addition, down-regulation of iNOS caused by andrographolide was also diminished by a 30-min pretreatment of okadaic acid at 10 nM in LPS/IFN-γ-stimulated rat VSMCs. (Fig. 5*B*). To further confirm more specifically that andrographolide's inhibitory actions on LPS/IFN-γ-induced iNOS expression and p65 Ser$^{536}$ phosphorylation was mediated by PP2A, *pp2a* siRNA was used. As shown in Fig. 5*C*, transfection of rat VSMCs with *pp2a* siRNA significantly reduced andrographolide-decreased iNOS expression in LPS/IFN-γ-stimulated rat VSMCs. Andrographolide-induced p65 Ser$^{536}$ dephosphorylation was also inhibited by *pp2a* siRNA (Fig. 5*D*). Furthermore, siRNA experiments revealed that *pp2a* siRNA suppressed the basal level of the PP2A catalytic subunit (PP2A-C) (Fig. 5*E*). Transfection of rat VSMCs with *pp2a* siRNA also significantly recovered from the andrographolide-induced inhibition of NF-κB-luciferase activity in LPS/IFN-γ-stimulated rat VSMCs (Fig. 6*A*). Stimulation of cells with 50 μM andrographolide time-dependently induced an increase of PP2A activity (Fig. 6*B*). A marked reduction in PP2A enzyme activity observed in rat VSMCs pretreated with 10 nM okadaic acid for 30 min (Fig. 6*B*) authenticated the effects of the PP2A inhibitor. Furthermore, the PP2A enzyme activity associated with a control immunoprecipitation using normal mouse IgG was 164.5 ± 50.6 pmol of phosphate/min (data not shown). These results suggest that PP2A may be specifically responsible for andrographolide-induced p65 Ser$^{536}$ dephosphorylation and subsequent iNOS down-regulation in rat VSMCs exposed to LPS and IFN-γ.

*Neutral Sphingomyelinase (nSMase) Is Involved in Andrographolide Attenuation of p65 Ser$^{536}$ Phosphorylation and iNOS Expression in LPS/IFN-γ-stimulated Rat VSMCs*—The precise mechanism involved in andrographolide-induced PP2A activation in rat VSMCs remains unclear. PP2A, a member of the ceramide-activated protein phosphatase family, is known to be activated by ceramide. We thus determined whether andrographolide induces ceramide formation in rat VSMCs. As shown in Fig. 7*A*, andrographolide time-dependently increased ceramide formation in rat VSMCs. Treatment of cells with 50 μM andrographolide for 30 min and/or 1 h significantly increased the ceramide level from 21.4 ± 2.0 to 41.9 ± 5.8 and 51.9 ± 11.2 ng/ml, respectively (Fig. 7*A*). In addition, andrographolide-induced ceramide formation was markedly attenuated by 3-OMe-SM (30 μM), an nSMase inhibitor (Fig. 7*B*). 3-OMe-SM was also used to determine whether nSMase is involved in the PP2A-p65-iNOS signaling cascade in response to andrographolide in LPS/IFN-γ-stimulated rat VSMCs. As shown in Fig. 7*C*, pretreatment with

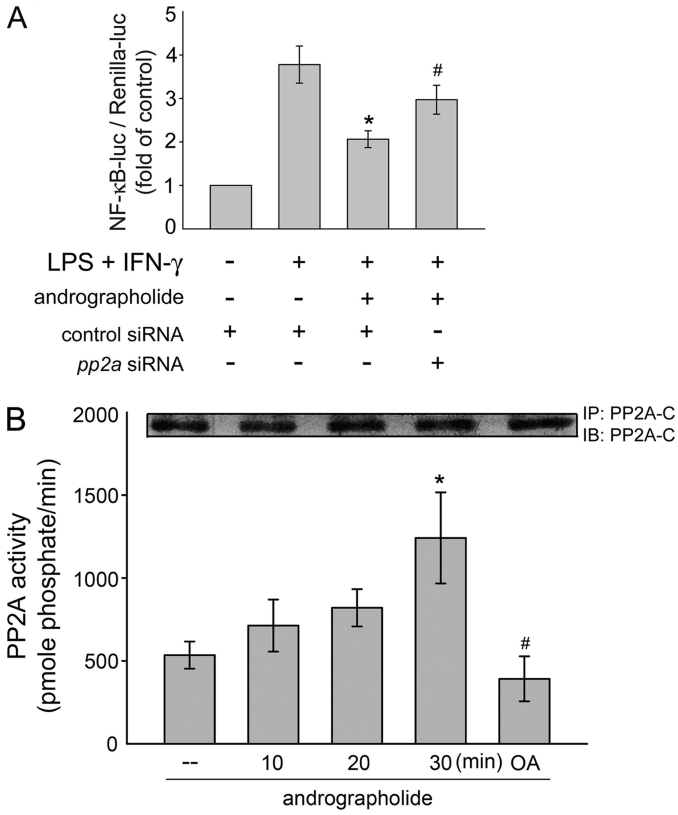


FIGURE 6. **Effects of andrographolide on PP2A activity in rat VSMCs.** *A*, cells were transiently transfected with NF-κB-luc and *Renilla*-luc and control siRNA or *pp2a* siRNA for 24 h. After transfection, cells were pretreated with vehicle or andrographolide for 30 min before treatment with the combination of LPS (50 μg/ml) and IFN-γ (100 units/ml) for another 24 h. An NF-κB-luciferase assay was then carried out. Data represent means ± S.E. (*error bars*) of four independent experiments performed in duplicate. *B*, PP2A activity was determined as described under "Experimental Procedures." Each column represents the mean ± S.E. of four independent experiments. *, $p < 0.05$, compared with the control group. #, $p < 0.05$, compared with the group in the presence of andrographolide at the 30 min time point. *IP*, immunoprecipitation; *IB*, immunoblotting.

3-OMe-SM for 30 min at a concentration of 30 μM significantly inhibited andrographolide-induced PP2A activation. Pretreatment with 3-OMe-SM also restored andrographolide inhibition of p65 Ser$^{536}$ phosphorylation in cells exposed to LPS/IFN-γ (Fig. 7*D*). In addition, down-regulation of iNOS caused by andrographolide was also diminished by a 30-min pretreatment of 3-OMe-SM in LPS/IFN-γ-stimulated rat VSMCs. (Fig. 7*E*). These results suggest that the nSMase-ceramide-PP2A cascade mediates andrographolide-induced p65 Ser$^{536}$ dephosphorylation and subsequent iNOS down-regulation in rat VSMCs exposed to LPS and IFN-γ.

*Effect of Andrographolide on Neointimal Formation and iNOS Expression in Rat Carotid Arteries*—It is well known that NF-κB activation and subsequent inflammatory gene expressions play crucial roles in the initiation and progression of neointimal formation by controlling vascular remodeling in

FIGURE 5. **PP2A is involved in andrographolide attenuation of NF-κB activity.** Cells were treated with okadaic acid (1–10 nM) (*A* and *B*) or transiently transfected with *pp2a* siRNA (*C*–*E*) followed by 30 min of treatment with andrographolide. After treatment, cells were treated with the combination of LPS (50 μg/ml) and IFN-γ (100 units/ml) for another 30 min (*A* and *C*) or 24 h (*B*, *D*, and *E*). The extent of p65 Ser$^{536}$ phosphorylation (*A* and *C*), iNOS (*B* and *D*), or PP2A catalytic subunit (PP2A-C) (*E*) was then determined. Data are presented as means ± S.E. (*error bars*). *, $p < 0.05$, compared with the control group. #, $p < 0.05$, compared with the LPS/IFN-γ-treated group in the presence of andrographolide.

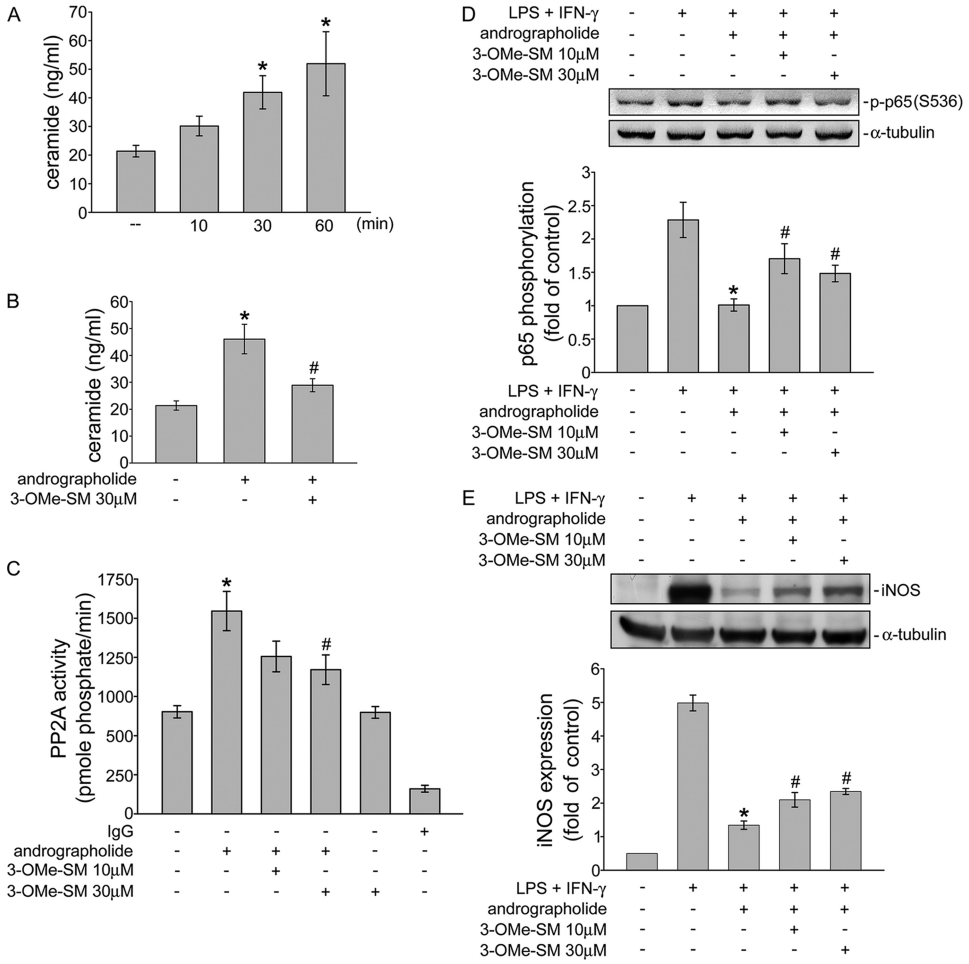


FIGURE 7. **nSMase is involved in andrographolide-induced ceramide formation and PP2A activation.** *A*, cells were treated with andrographolide (50 $\mu$M) for the indicated times. Ceramide levels were then determined as described under "Experimental Procedures." Each *column* represents the mean ± S.E. (*error bar*) of three independent experiments. *, $p < 0.05$, compared with the control group. *B*, cells were pretreated with vehicle or 3-OMe-SM (30 $\mu$M) for 30 min before treatment with andrographolide (50 $\mu$M) for another 30 min. Ceramide levels were then determined as described under "Experimental Procedures." Each *column* represents the mean ± S.E. of three independent experiments. *, $p < 0.05$, compared with the control group. #, $p < 0.05$, compared with the group treated with andrographolide alone. *C*, cells were pretreated with vehicle or 3-OMe-SM (10–30 $\mu$M) for 30 min before treatment with andrographolide (50 $\mu$M) for another 30 min. PP2A activity was then determined. Each *column* represents the mean ± S.E. of four independent experiments. *, $p < 0.05$, compared with the control group. #, $p < 0.05$, compared with the group treated with andrographolide alone. Cells were treated with 3-OMe-SM (10–30 $\mu$M) followed by a 30-min treatment with andrographolide. After treatment, cells were treated with the combination of LPS (50 $\mu$g/ml) and IFN-$\gamma$ (100 units/ml) for another 30 min (*D*) or 24 h (*E*). The extent of p65 $Ser^{536}$ phosphorylation (*D*) and/or iNOS expression (*E*) was then determined. Data are presented as means ± S.E. *, $p < 0.05$, compared with the vehicle-treated group. #, $p < 0.05$, compared with the LPS/IFN-$\gamma$-treated group in the presence of andrographolide.

response to various noxious stimuli (25). Based on the above findings that andrographolide may suppress LPS/IFN-$\gamma$-induced iNOS expression through PP2A-mediated NF-$\kappa$B inhibition in VSMCs, we thus investigated whether andrographolide may inhibit vascular inflammation-associated neointimal formation. Using a rat carotid injury model, we found a remarkable increase in neointimal formation at 14 days after balloon injury in control rats, which was significantly reduced in the andrographolide-treated group (5 mg/kg/day) (Fig. 8*A*). The intimal area/medial area ratio at 14 days in vehicle-treated rats was reduced from 1.7 ± 0.1 to 0.4 ± 0.2 by andrographolide treatment ($p < 0.05$, $n = 5$). In addition, iNOS expression was markedly increased in injured carotid arteries as compared with the normal carotid arteries (sham control). The increased iNOS expression at 14 days after balloon injury was significantly reduced in andrographolide-treated rats as compared with vehicle-treated rats (Fig. 8*B*) (sham control, 1.0 ± 0.0-fold; balloon-injured plus vehicle, 3.9 ± 0.2-fold; balloon-injured plus 50 $\mu$M andrographolide, 2.5 ± 0.5-fold; $p < 0.05$, $n = 3$). These data suggest that andrographolide may improve vascular inflammatory disease-associated neointimal formation, such as atherosclerosis.

## DISCUSSION

Andrographolide was recently shown to inhibit the expression of inflammatory mediators in macrophages and lung epithelial cells under inflammatory stimuli (14–16). Bao *et al.* (14) also demonstrated that andrographolide may possess anti-inflammatory activities and the therapeutic potential to treat allergic asthma. In the present study, in an effort to increase the therapeutic potential use of andrographolide in cardiovascular diseases, andrographolide was shown to inhibit LPS/IFN-$\gamma$-induced iNOS and MMP-9 expressions in rat VSMCs and to reduce neointimal formation in a rat carotid

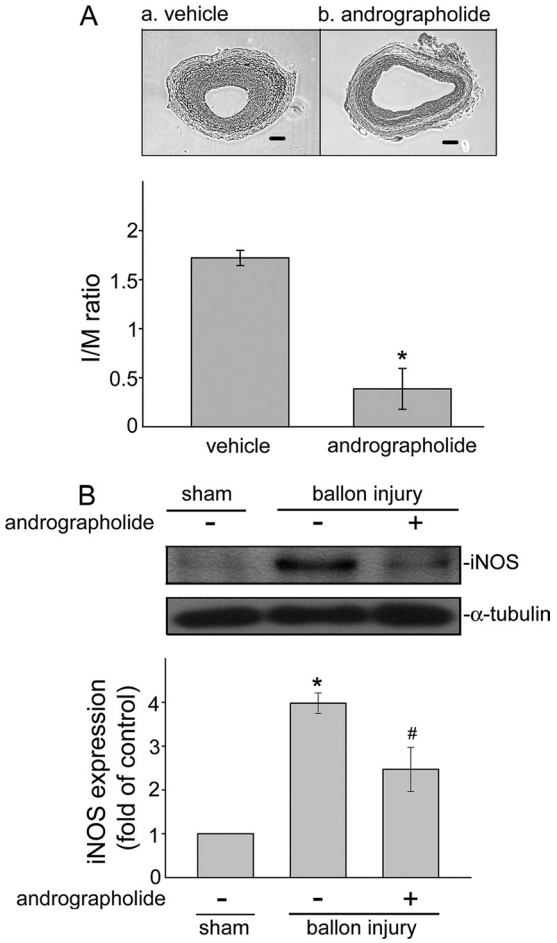


FIGURE 8. **Effects of andrographolide on neointimal formation and iNOS expression in a rat carotid injury model.** *A*, photomicrographs showing the effect of andrographolide (5 mg/kg/day) (*b*) on neointimal formation in rat carotid arteries of 14 days after balloon injury (magnification ×400). Results are presented as means ± S.E. (*error bars*). *, $p < 0.05$, compared with the vehicle-treated balloon injury group (*a*). *I/M*, intimal area/medial area. *B*, uninjured (sham) and injured rat carotid arteries 14 days after balloon injury in vehicle- or andrographolide-treated rats (5 mg/kg/day) were harvested and subjected to Western blotting to determine iNOS level. Data are presented as means ± S.E. *, $p < 0.05$, compared with the sham group. #, $p < 0.05$, compared with the vehicle-treated balloon injury group.

injury model. This study also demonstrated for the first time that PP2A dephosphorylation of the p65 subunit of NF-κB may contribute to andrographolide's protective actions in rat VSMCs.

Several lines of evidence have demonstrated that NF-κB plays a crucial role in andrographolide's anti-inflammatory actions (15, 16). However, the precise molecular mechanism by which andrographolide attenuates NF-κB remains incompletely characterized. The common form of NF-κB in most cell types is the p65/p50 heterodimer, and NF-κB signaling is tightly controlled by the IKK complex, which consists of IKKα, IKKβ, and IKKγ together with its downstream substrate IκBα. Upon stimulation, the activated IKK phosphorylates IκBα, leading to IκBα degradation and enhanced NF-κB nuclear translocation and subsequent transcriptional activation (33). Results from the present study, similar to those reported previously (15, 16), show that andrographolide reduced nuclear translocation of NF-κB and diminished NF-κB binding to DNA. Wang *et al.* (15) further demonstrated that andrographolide covalently modified the reduced cysteine 62 of p50, and andrographolide did not further reduce NF-κB-mediated neointimal formation in $p50^{-/-}$ mice (16). Those studies suggested the specificity of andrographolide for p50. Whether p65 contributes to andrographolide's inhibition of NF-κB has not previously been demonstrated. We showed in the present study that p65 was dephosphorylated and causally related to andrographolide's attenuation of NF-κB signaling. In addition, phosphorylation of p65 at $Ser^{536}$, but not at $Ser^{276}$, was altered in the presence of andrographolide in LPS/IFN-γ-stimulated rat VSMCs.

NF-κB activation is tightly controlled to ensure a functioning host defense and prevent hyperinflammation and tumorigenesis (27). In addition to IκB, the phosphorylation of the NF-κB subunit p65 represents another mechanism regulating NF-κB nuclear imports, exports, and transcriptional activities. Previous studies postulated that phosphorylation of p65 up-regulates NF-κB-dependent transcription (27). We showed that dephosphorylation of p65 may be causally related to andrographolide's inhibitory actions on NF-κB in LPS/IFN-γ-stimulated rat VSMCs. The molecular mechanism involved in p65 $Ser^{536}$ dephosphorylation by andrographolide remains unresolved. IKK was previously shown to phosphorylate p65 at $Ser^{536}$ (31), and andrographolide was reported to suppress p65 $Ser^{536}$ phosphorylation through IKK inhibition in lung epithelial cells (14). However, andrographolide did not affect IKK activation in rat VSMCs, as demonstrated in the present study. Activation of an unknown protein phosphatase is thus postulated to be required for andrographolide's attenuation of NF-κB activity by dephosphorylating p65 $Ser^{536}$. A number of studies demonstrated that PP2A can regulate the activation of NF-κB (34). In agreement with those observations, we noted that okadaic acid, a specific inhibitor of PP2A, inhibited andrographolide dephosphorylation of p65 $Ser^{536}$ residues and subsequent iNOS expression. Furthermore, *pp2a* siRNAs, which silenced PP2A-C, also attenuated andrographolide dephosphorylation of p65 $Ser^{536}$. Andrographolide also induced PP2A activation in rat VSMCs. These findings suggest that PP2A plays a pivotal role in andrographolide's actions in an IKK-independent manner in rat VSMCs.

Previous studies have demonstrated that the formation of ceramide catalyzed by nSMase plays a critical role in PP2A activation (35, 36). In agreement with these observations, we noted that 3-OMe-SM, a specific inhibitor of nSMase, inhibited andrographolide-induced ceramide formation and PP2A activation. Andrographolide mediated dephosphorylation of p65 $Ser^{536}$ residues and subsequent iNOS expression were also attenuated by 3-OMe-SM in LPS/IFN-γ-stimulated rat VSMCs. Taken together, these findings suggest that the nSMase-ceramide cascade mediated andrographolide-induced PP2A activation in rat VSMCs. In addition, ceramide may be derived from sphingomyelin hydrolysis catalyzed by either nSMase or acidic sphingomyelinase (37). Another pathway involves ceramide synthase-catalyzed *de novo* ceramide syn-

thesis (38). However, further investigations are needed to characterize whether acidic sphingomyelinase or *de novo* ceramide synthesis contributes to andrographolide-induced ceramide formation and subsequent PP2A activation in rat VSMCs.

In addition to NF-κB, activator protein (AP)-1 may also contribute to iNOS (9) and MMP-9 (39) expressions in VSMCs. In our preliminary studies in rat VSMCs, AP-1 was also a candidate targeted by andrographolide to down-regulate iNOS and MMP-9 expressions. We found that andrographolide significantly suppressed JNK phosphorylation and diminished AP-1 reporter activity in LPS/IFN-γ-stimulated rat VSMCs.[4] JNK, a critical upstream molecule of AP-1, was also shown to be negatively regulated by PP2A (40). Together, these findings raise the possibility that andrographolide's activation of PP2A may regulate at least two separate pathways: one on the JNK-AP-1 cascade and another on the p65 cascade as reported here. The different mechanisms of andrographolide's actions in driving these two signaling pathways downstream of PP2A remain to be elucidated. It is likely that the two pathways may culminate in decreasing iNOS and MMP-9 expressions.

NO is an important regulator of vascular function. Several lines of evidence demonstrated that NO-derived oxidant peroxynitrite contributes to inflammatory cardiovascular diseases, such as atherogenesis (9). In addition, MMPs also play important roles in vascular remodeling and subsequent pathological events in the progression of diabetes, coronary arterial diseases, and atherosclerosis (41). Because NF-κB is a critical transcription factor in transactivating inflammatory genes, including iNOS and MMP-9, it appears to be a promising molecular target in treating inflammatory vascular diseases. Various therapeutic strategies targeted at the NF-κB signaling pathway, such as NF-κB-specific decoy oligonucleotide (42) and IKKβ-selective small molecule inhibitor (43), have demonstrated beneficial effects in experimental inflammatory animal models. Our findings revealed that andrographolide significantly diminished iNOS and MMP-9 expressions in LPS/IFN-γ-stimulated rat VSMCs. We also demonstrated for the first time that andrographolide inhibited p65 $Ser^{536}$ phosphorylation, reduced nuclear translocation of p65, and diminished p65 κB oligonucleotide binding in LPS/IFN-γ-stimulated rat VSMCs. In addition, PP2A may contribute to these actions of andrographolide in rat VSMCs. Results from the rat carotid injury model also demonstrated that andrographolide had beneficial effects in inhibiting balloon injury-induced neointimal formation and iNOS expression. Taken together, these findings support a therapeutic value for andrographolide in treating inflammatory vascular diseases.

## REFERENCES


1. McKellar, G. E., McCarey, D. W., Sattar, N., and McInnes, I. B. (2009) *Nat. Rev. Cardiol.* **6,** 410–417
2. Yang, Z., Gagarin, D., St Laurent, G., 3rd, Hammell, N., Toma, I., Hu, C. A., Iwasa, A., and McCaffrey, T. A. (2009) *Arterioscler. Thromb. Vasc. Biol.* **29,** 1213–1219
3. Frantz, S., Ertl, G., and Bauersachs, J. (2007) *Nat. Clin. Pract. Cardiovasc. Med.* **4,** 444–454
4. Boos, C. J., Goon, P. K., and Lip, G. Y. (2006) *Clin. Pharmacol. Ther.* **79,** 20–22
5. Cartwright, N., Murch, O., McMaster, S. K., Paul-Clark, M. J., van Heel, D. A., Ryffel, B., Quesniaux, V. F., Evans, T. W., Thiemermann, C., and Mitchell, J. A. (2007) *Am. J. Respir. Crit. Care. Med.* **175,** 595–603
6. Bogdan, C. (2001) *Nat. Immunol.* **2,** 907–916
7. Parrillo, J. E. (1993) *N. Engl. J. Med.* **328,** 1471–1477
8. Jeremy, J. Y., Rowe, D., Emsley, A. M., and Newby, A. C. (1999) *Cardiovasc. Res.* **43,** 580–594
9. Hattori, Y., Matsumura, M., and Kasai, K. (2003) *Cardiovasc. Res.* **58,** 186–195
10. Negi, A. S., Kumar, J. K., Luqman, S., Shanker, K., Gupta, M. M., and Khanuja, S. P. (2008) *Med. Res. Rev.* **28,** 746–772
11. Zhou, J., Lu, G. D., Ong, C. S., Ong, C. N., and Shen, H. M. (2008) *Mol. Cancer Ther.* **7,** 2170–2180
12. Iruretagoyena, M. I., Tobar, J. A., González, P. A., Sepúlveda, S. E., Figueroa, C. A., Burgos, R. A., Hancke, J. L., and Kalergis, A. M. (2005) *J. Pharmacol. Exp. Ther.* **312,** 366–372
13. Chiou, W. F., Chen, C. F., and Lin, J. J. (2000) *Br. J. Pharmacol.* **129,** 1553–1560
14. Bao, Z., Guan, S., Cheng, C., Wu, S., Wong, S. H., Kemeny, D. M., Leung, B. P., and Wong, W. S. (2009) *Am. J. Respir. Crit. Care. Med.* **179,** 657–665
15. Xia, Y. F., Ye, B. Q., Li, Y. D., Wang, J. G., He, X. J., Lin, X., Yao, X., Ma, D., Slungaard, A., Hebbel, R. P., Key, N. S., and Geng, J. G. (2004) *J. Immunol.* **173,** 4207–4217
16. Wang, Y. J., Wang, J. T., Fan, Q. X., and Geng, J. G. (2007) *Cell Res.* **17,** 933–941
17. Hsiao, G., Shen, M. Y., Chang, W. C., Cheng, Y. W., Pan, S. L., Kuo, Y. H., Chen, T. F., and Sheu, J. R. (2003) *Biochem. Pharmacol.* **65,** 1383–1392
18. Beasley, D., Schwartz, J. H., and Brenner, B. M. (1991) *J. Clin. Invest.* **87,** 602–608
19. Hsu, M. J., Lee, S. S., and Lin, W. W. (2002) *J. Leukoc. Biol.* **72,** 207–216
20. Hsu, M. J., Hsu, C. Y., Chen, B. C., Chen, M. C., Ou, G., and Lin, C. H. (2007) *J. Neurosci.* **27,** 5719–5729
21. Schiffmann, S., Sandner, J., Schmidt, R., Birod, K., Wobst, I., Schmidt, H., Angioni, C., Geisslinger, G., and Grösch, S. (2009) *J. Lipid Res.* **50,** 32–40
22. Lanone, S., Zheng, T., Zhu, Z., Liu, W., Lee, C. G., Ma, B., Chen, Q., Homer, R. J., Wang, J., Rabach, L. A., Rabach, M. E., Shipley, J. M., Shapiro, S. D., Senior, R. M., and Elias, J. A. (2002) *J. Clin. Invest.* **110,** 463–474
23. Newby, A. C. (2006) *Cardiovasc. Res.* **69,** 614–624
24. Hattori, Y., Kasai, K., and Gross, S. S. (2004) *Cardiovasc. Res.* **63,** 31–40
25. Lee, C. S., Kwon, Y. W., Yang, H. M., Kim, S. H., Kim, T. Y., Hur, J., Park, K. W., Cho, H. J., Kang, H. J., Park, Y. B., and Kim, H. S. (2009) *Arterioscler. Thromb. Vasc. Biol.* **29,** 472–479
26. Karin, M. (2006) *Nature* **441,** 431–436
27. Ghosh, S., and Karin, M. (2002) *Cell* **109,** (suppl.) S81–S96
28. Belaiba, R. S., Bonello, S., Zähringer, C., Schmidt, S., Hess, J., Kietzmann, T., and Görlach, A. (2007) *Mol. Biol. Cell* **18,** 4691–4697
29. Li, Q., and Verma, I. M. (2002) *Nat. Rev. Immunol.* **2,** 725–734
30. Zhong, H., Voll, R. E., and Ghosh, S. (1998) *Mol. Cell* **1,** 661–671
31. Sakurai, H., Chiba, H., Miyoshi, H., Sugita, T., and Toriumi, W. (1999) *J. Biol. Chem.* **274,** 30353–30356
32. Hunter, T. (2000) *Cell* **100,** 113–127
33. Perkins, N. D. (2007) *Nat. Rev. Mol. Cell Biol.* **8,** 49–62
34. Li, S., Wang, L., Berman, M. A., Zhang, Y., and Dorf, M. E. (2006) *Mol. Cell* **24,** 497–509
35. Lee, J. T., Xu, J., Lee, J. M., Ku, G., Han, X., Yang, D. I., Chen, S., and Hsu, C. Y. (2004) *J. Cell Biol.* **164,** 123–131
36. Chen, B. C., Chang, H. M., Hsu, M. J., Shih, C. M., Chiu, Y. H., Chiu, W. T., and Lin, C. H. (2009) *J. Biol. Chem.* **284,** 20562–20573
37. Testi, R. (1996) *Trends Biochem. Sci.* **21,** 468–471
38. Xu, J., Yeh, C. H., Chen, S., He, L., Sensi, S. L., Canzoniero, L. M., Choi,


[4] C. Y. Hsieh, M. J. Hsu, G. Hsiao, Y. H. Wang, C. W. Huang, S. W. Chen, T. Jayakumar, P. T. Chiu, Y. H. Chiu, and J. R. Sheu, unpublished data.

D. W., and Hsu, C. Y. (1998) *J. Biol. Chem.* **273,** 16521–16526
39. Chandrasekar, B., Mummidi, S., Mahimainathan, L., Patel, D. N., Bailey, S. R., Imam, S. Z., Greene, W. C., and Valente, A. J. (2006) *J. Biol. Chem.* **281,** 15099–15109
40. Kins, S., Kurosinski, P., Nitsch, R. M., and Götz, J. (2003) *Am. J. Pathol.* **163,** 833–843
41. Chung, A. W., Yang, H. H., Sigrist, M. K., Brin, G., Chum, E., Gourlay, W. A., and Levin, A. (2009) *Cardiovasc. Res.* **84,** 494–504
42. Desmet, C., Gosset, P., Pajak, B., Cataldo, D., Bentires-Alj, M., Lekeux, P., and Bureau, F. (2004) *J. Immunol.* **173,** 5766–5775
43. Birrell, M. A., Hardaker, E., Wong, S., McCluskie, K., Catley, M., De Alba, J., Newton, R., Haj-Yahia, S., Pun, K. T., Watts, C. J., Shaw, R. J., Savage, T. J., and Belvisi, M. G. (2005) *Am. J. Respir. Crit. Care. Med.* **172,** 962–971